Acta Crystallographica Section B
Structural Science
ISSN 0108-7681

Modulated corrugations in the crystal structure of the superconductor CaAlSi

Karine M. Sparta,[a]* Ralf Müller,[a,b] Michael Merz,[a] Georg Roth,[a] Peter Adelmann[c] and Thomas Wolf[c]

[a]Institut für Kristallographie der RWTH Aachen, Jägerstraße 17-19, 52056 Aachen, Germany, [b]Carl Zeiss SMT AG, Carl-Zeiss-Straße 22, 73447 Oberkochen, Germany, and [c]Forschungszentrum Karlsruhe, Institut für Festkörperphysik, PO Box 3640, 76021 Karlsruhe, Germany

Correspondence e-mail: sparta@xtal.rwth-aachen.de

Received 25 January 2006
Accepted 5 July 2006

We report the crystal structure analyses of CaAlSi from single-crystal and powder X-ray diffraction and the existence of two commensurately modulated phases, a sixfold and a fivefold modulated structure. This polymorphism seems to be correlated to the thermal history of the sample. We describe both modulated structures using a three-dimensional and a (3 + 1)-dimensional formalism.

1. Introduction

Since the recent discovery of superconductivity at 39 K in the intermetallic compound MgB_2 [space group $P6/mmm$ (191), $a = 3.086$, $c = 3.524$ Å] by Nagamatsu *et al.* (2001), materials with layered crystal structures similar to that of AlB_2 have been investigated as possible candidates for new high-T_c superconductors. According to an extensive study by Hoffmann & Pöttgen (2001), 46 structure types of binary and ternary intermetallic compounds can be derived from the structure of AlB_2, including more than 1500 compounds, but the search for high-T_c materials has been mostly focused on binary and ternary silicides. Among those, β-$ThSi_2$ is known to become a superconductor at $T_c \simeq 2.4$ K (Hardy & Hulm, 1954), and $CaSi_2$ is superconducting with onset temperatures up to $T_c = 14$ K, although only under high pressure (MacWhan *et al.*, 1967; Bordet *et al.*, 2000; Sanfilippo *et al.*, 2000). More recently, ternary silicides of composition $AX_{2-x}Si_x$ were synthesized and investigated, with A = Ca, Sr, Ba and X = Ga, Al (Imai, Nishida, Kimura & Abe, 2002; Imai, Nishida, Kimura, Kitazawa *et al.*, 2002; Lorenz *et al.*, 2002). It was reported that $CaAl_{2-x}Si_x$ crystallizes in the AlB_2-type structure for $0.6 \leq x \leq 1.5$, with a possible miscibility gap around $x = 1.1$. Within this range of compositions, the highest T_c was obtained for $Ca(Al_{0.5}Si_{0.5})_2$, or CaAlSi, with $T_c \simeq 7.7$ K.

We report crystal structure determinations of CaAlSi from single-crystal and powder X-ray diffraction and the existence of two commensurately modulated structures, depending on the cooling rate of the crystals during the synthesis. Similar observations from single-crystal X-ray diffraction have been reported by Tamegai *et al.* (2005), but without any reference to the crystal structure.

2. Experimental

2.1. Crystal growth

Two different batches of CaAlSi were prepared for the single-crystal X-ray diffraction measurements by melting stoichiometric amounts of Al (Koch Light, powder), Ca (Alfa, 2N5, granules) and Si (Roth, 5N, powder) under an inert

Table 1
Subcell of CaAlSi: lattice parameters and volume at different temperatures from X-ray powder diffraction measurements.

Temperature (K)	a_0 (Å)	c_0 (Å)	V_0 (Å^3)
328	4.17811 (5)	4.39071 (7)	66.378 (3)
298	4.17720 (4)	4.38744 (6)	66.300 (2)
260	4.17648 (4)	4.38440 (5)	66.231 (2)
230	4.17571 (4)	4.38113 (5)	66.157 (2)
200	4.17469 (3)	4.37760 (4)	66.072(2)
170	4.17367 (4)	4.37446 (5)	65.992 (2)
140	4.17302 (4)	4.37166 (5)	65.929 (2)
110	4.17250 (4)	4.36900 (5)	65.873 (2)
80	4.17198 (4)	4.36655 (5)	65.819 (2)
50	4.17190 (4)	4.36524 (5)	65.797 (2)
20	4.17190 (4)	4.36505 (5)	65.794 (2)

atmosphere of 1 bar Ar. Sample (1) was melted in a tungsten crucible in an induction furnace at 1373 K and, after 10 min, quenched in air at a rate of > 50 K min^{-1}. Sample (2) was prepared in an Al_2O_3 crucible enclosed in an Al_2O_3 tube in a horizontal tubular furnace. The heating rate was 4.2 K min^{-1} up to 1273 K, where the sample was kept for 24 min. The sample was then cooled to 1229 K at a rate of 0.04 K min^{-1}, and finally quenched to room temperature by pulling the Al_2O_3 tube out of the furnace. The estimated cooling rate during the last step was about 20 K min^{-1}. A part of sample (2) was further annealed under Ar at 1173 K over a period of 7 h and then cooled to room temperature at a rate of 5.8 K min^{-1}. All three samples are superconductors, with T_c of 8.20, 7.37 and 6.98 K, respectively (measured inductively, midpoint T_c). The T_c of sample (1) is significantly higher than the value given in the literature.

For the X-ray powder diffraction analysis a polycrystalline sample was prepared by weighing and pressing a stoichiometric amount of Al, Ca and Si. This pellet was arc melted in an atmosphere of 600 mbar Ar(6.0) with subsequent rapid quenching on a copper plate (cooling rate about 600 K min^{-1}).

2.2. Powder X-ray diffraction

In order to determine the lattice parameters of CaAlSi a high-resolution X-ray powder diffractometer (X'Pert PRO PANalytical) was applied. The data were collected in Bragg–Brentano geometry using Cu $K\alpha_{1,2}$ radiation and tube settings of 45 kV and 40 mA. Owing to the θ–θ geometry of the diffractometer the flat sample was fixed in the horizontal plane. The sample holder consisted of a Cu plate mounted on top of a double-stage closed-cycle cooler. The temperature of the sample was controlled by two diode sensors and had a stability of ± 0.1 K. One sensor was in direct contact with the sample holder, and the other was situated close to the heater at the cold-head. To keep intensity losses and background scattering as low as possible, the cryostat was equipped with low-absorbing Mylar X-ray windows. Eventually, the beam was diffracted onto a position-sensitive solid-state detector (PANalytical X'Celerator).

The powder sample itself was finely ground from CaAlSi polycrystals. Small amounts of oxidized material (of pale green colour), however, could not be separated from the bulk. Eleven diffraction patterns were measured during heating from 20 up to 328 K. The temperature of the sample was stabilized for about 10 min after each change. We used the following data collection strategy: For each temperature, a powder diffraction pattern was measured between 15 and 95° in 2θ within 1 h. 20 such patterns were collected and combined together to produce a single data file. Throughout the measurements, silicon powder was employed as an internal standard to ensure a high accuracy for the determination of the cell parameters and to compensate for the temperature-dependent displacement errors. The lattice parameter of silicon was taken from earlier calibration measurements, and the cell parameters of CaAlSi (Table 1) were obtained from pattern matching refinements using the program *FULLPROF* (Rodriguez-Carvajal, 2005).

2.3. Single crystal X-ray diffraction

The samples used for these measurements were small pieces that we cut from the larger crystals, of dark grey metallic colour. It should be noted that no trace of the pale green oxidized material could be seen on these pieces.

A data set was collected with a $0.15 \times 0.16 \times 0.18$ mm^3 single crystal of CaAlSi from sample (2) (sixfold superstructure) at 298 K, on a Stoe IPDS II imaging plate diffractometer (Mo $K\alpha$ radiation, pyrolytic graphite monochromator). The intensity data were collected with an ω oscillation movement between 0 and 180° for $\varphi = 15°$; the ω rotation during exposure was 0.5° per frame. The data set was collected with a tube setting of 30 kV and 25 mA in order to avoid the presence of the $\lambda/2$ radiation, an exposure time of 16 min per frame in order to obtain good statistics on the intensities of the superstructure reflections, and a sample–detector distance of 120 mm.

A data set was collected with a $0.18 \times 0.20 \times 0.21$ mm^3 single crystal of CaAlSi from the annealed sample (2) (fivefold superstructure) on the same diffractometer. The crystals from sample (1) also show a fivefold superstructure, but their analysis will not be discussed here because it leads to the same results. In particular, the cell parameters for sample (1) and annealed sample (2) agree within three standard deviations. The intensity data were collected with an ω oscillation movement between 0 and 180° for $\varphi = 0$ and 0°; the ω rotation during exposure was 1° per frame. We used a tube setting of 50 kV and 25 mA because the $\lambda/2$ radiation does not interfere with the fivefold superstructure. The data set was collected with an exposure time of 15 min per frame; the sample–detector distance was 100 mm. We also collected a data set at 100 K with this crystal, but apart from the cell parameters, the structure does not change significantly.

The lattice parameters and the intensities of the reflections for the single-crystal data sets were obtained with the program

Table 2
Experimental and refinement details for the single-crystal measurements.

	Sixfold superstructure	Fivefold superstructure
Crystal data		
Chemical formula	AlSiCa	AlSiCa
M_r	95.15	95.15
Cell setting, space group	Hexagonal, $P\bar{6}m2$	Hexagonal, $P\bar{6}m2$
Temperature (K)	298	298
a, c (Å)	4.17720 (4), 26.3246 (4)	4.17720 (4), 21.9372 (3)
V (Å^3)	397.80 (1)	331.50 (1)
Z	6	5
D_x (Mg m^{-3})	2.383	2.383
Radiation type	Mo $K\alpha$	Mo $K\alpha$
μ (mm^{-1})	2.76	2.76
Crystal form, colour	Cuboid, metallic dark grey	Cuboid, metallic dark grey
Crystal size (mm)	0.18 × 0.16 × 0.15	0.21 × 0.20 × 0.18
Data collection		
Diffractometer	Stoe IPDS-II	Stoe IPDS-II
Data collection method	ω scans	ω scans
Absorption correction	Empirical (using intensity measurements)	Empirical (using intensity measurements)
T_{min}	0.557	0.531
T_{max}	0.660	0.607
No. of measured, independent and observed reflections	3136, 429, 233	4754, 422, 340
Criterion for observed reflections	$I > 2\sigma(I)$	$I > 2\sigma(I)$
R_{int}	0.049	0.058
θ_{max} (°)	27.1	29.2
Refinement		
Refinement on	F^2	F^2
$R[F^2 > 2\sigma(F^2)]$, $wR(F^2)$, S	0.03, 0.082, 1.96	0.035, 0.086, 1.99
No. of reflections	429	422
No. of parameters	31	26
H-atom treatment	No H atoms present	No H atoms present
Weighting scheme	$w = 1/[\sigma^2(F_o^2) + (0.013P)^2]$, where $P = (F_o^2 + 2F_c^2)/3$	$w = 1/[\sigma^2(F_o^2) + (0.023P)^2]$, where $P = (F_o^2 + 2F_c^2)/3$
$(\Delta/\sigma)_{max}$	<0.0001	<0.0001
$\Delta\rho_{max}$, $\Delta\rho_{min}$ (e Å^{-3})	0.25, −0.28	0.46, −0.41
Absolute structure	Flack (1983)	Flack (1983)
Flack parameter	0.1 (3)	0.5 (4)

Computer programs used: *X-AREA* (Stoe & Cie, 2002), *FullProf Suite* (Rodriguez-Carvajal, 2005), *X-RED* (Stoe & Cie, 1996), *SHELXL97* (Sheldrick, 1997), *ATOMS* (Dowty, 2000), *WinGX* (Version 1.64.05; Farrugia, 1999).

X-AREA (Stoe & Cie, 2002), which was also used to reconstruct the planes of the reciprocal space. Empirical absorption corrections *via* symmetry equivalents were performed using the programs *X-RED* and *X-SHAPE* (Stoe & Cie, 1996). The structures were solved and refined with the program *SHELXL97* (Sheldrick, 1997), as implemented in the program suite *WinGX* (Version 1.64.05; Farrugia, 1999). Refinements for the superspace models were performed with the program *JANA2000* (Petricek *et al.*, 2000). Details are summarized in Table 2).[1]

[1] Supplementary data for this paper are available from the IUCr electronic archives (Reference: CK5016). Services for accessing these data are described at the back of the journal.

3. Results

3.1. Powder X-ray diffraction

Because of the presence of oxidized material, the weakness of the superstructure reflections, and the possible coexistence of both sixfold and fivefold superstructures within the sample, the pattern matching refinements were performed only to determine the temperature dependence of the cell parameters of the average structure. Fig. 1 shows a part of the measured diffraction pattern at room temperature between 23 and 31° in 2θ, as well as the corresponding simulation from the refined single-crystal structures using the profile parameters from the powder measurement. From the simulation, it follows that the superstructure reflections are too weak to be observed with X-ray powder diffraction; in fact, only the (105) reflection of the sixfold superstructure and the (104) reflection of the fivefold superstructure could, in principle, be observed. However, the presence of a peak from impurities just between those two reflections makes them useless for determining the cell parameters of the superstructures. The thermal expansion is higher in the direction perpendicular to the layers than within the layers (Fig. 2); above 100 K, α_{11} = 6.4 (2) × 10^{-6} K^{-1} and α_{33} = 2.32 (4) × 10^{-5} K^{-1}; below 100 K, α_{11} and α_{33} are zero to within three standard deviations. There is no indication of any structural phase transition down to 20 K.

3.2. Single-crystal X-ray diffraction

In earlier papers, it was assumed that CaAlSi has the AlB_2-type structure [space group $P6/mmm$, $a_0 = 4.1905\,(5)$ Å and $c_0 = 4.3992\,(8)$ Å at room temperature], consisting of strictly planar (Al,Si) layers orthogonal to the c axis and separated by Ca layers (Imai, Nishida, Kimura, Kitazawa *et al.*, 2002). The Ca atoms occupy the positions of the Al atoms in AlB_2, while the Al and Si atoms are equally distributed on the positions of

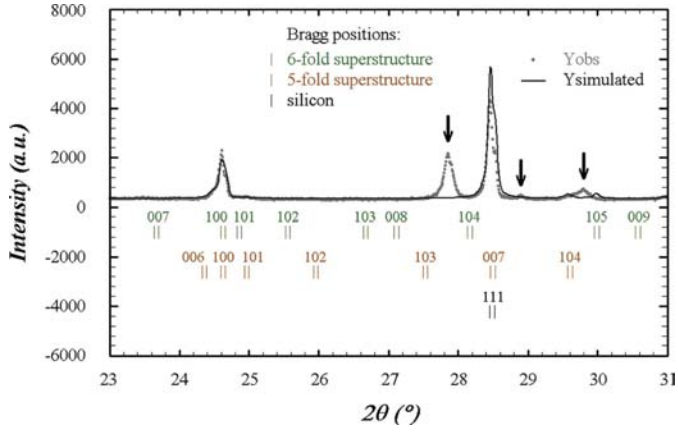

Figure 1
Part of the X-ray powder diffractogram of CaAlSi at room temperature. The Bragg positions for the six- and fivefold superstructures shown here were calculated from the pattern-matching refinements of the cell parameters of the average structure. The dotted line shows the measured diffractogram. The arrows point to peaks from oxidized material. The solid line represents the simulated diffractogram using the refined structures from single-crystal X-ray diffraction.

the B atoms, forming hexagonal six-membered rings. However, our single-crystal X-ray diffraction experiments, together with earlier observations of superstructure reflections at room temperature (Tamegai *et al.*, 2005), show that the unit cell of CaAlSi can be either five or six times larger in the *c* direction. An ordering of (Al–Si) distributions within the flat layers along the *c* axis is not likely to be responsible for the relatively high observed intensities of these new reflections since Al ($Z = 13$) and Si ($Z = 14$) have similar form factors. This clearly points to a modulation of atomic positions along *c*.

Whereas the crystals from the rapidly cooled sample (2) exhibit a sixfold superstructure (Fig. 3), the crystals from sample (1) and annealed sample (2) show a fivefold superstructure (Fig. 4). In the case of the sixfold superstructure, we also observe diffuse scattering around the Bragg peaks along the 2θ direction, indicating different d_{hkl} values and thus a more disordered state than in the case of the fivefold superstructure. The cell parameters of the two phases, as determined from the single-crystal diffraction measurements, differ slightly. The *a* parameter is shorter for the sixfold superstructure, while the *c* parameter, perpendicular to the (Si,Al) layers, is shorter for the fivefold superstructure. In the following, the average cell parameters obtained from powder diffraction are used for both superstructures.

3.2.1. Description in three dimensions. The determination of the correct space groups to describe these superstructures is

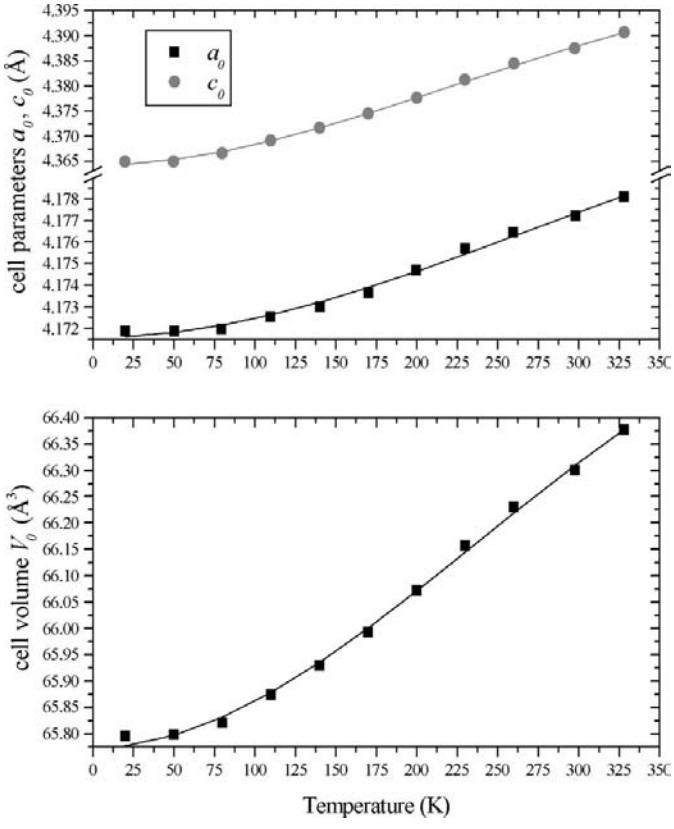

Figure 2
Temperature dependence of the cell parameters and volume of the subcell of CaAlSi. The error bars are contained within the point symbols. The third-order polynomial fits are guides to the eye.

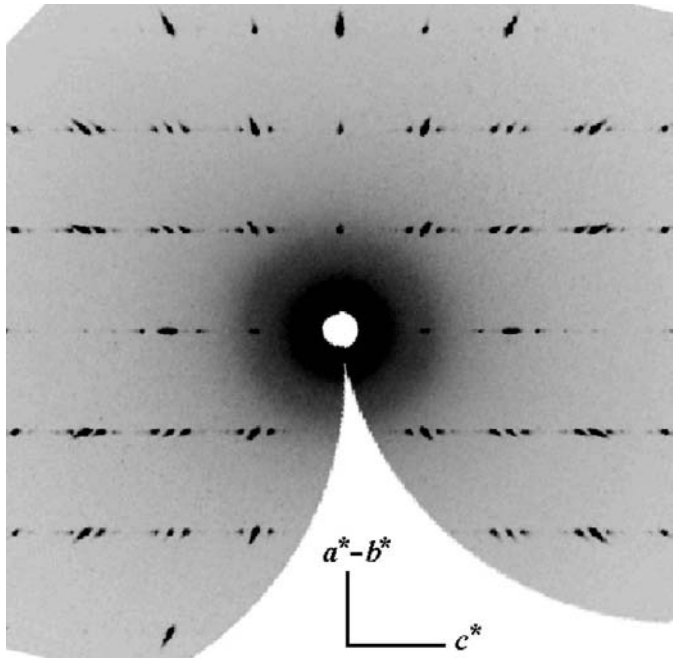

Figure 3
Reconstructed image of the ($h\bar{h}0l$) reciprocal plane of the sixfold superstructure of CaAlSi. The strong reflections correspond to the average structure with the symmetry $P6/mmm$; they are separated along the c^* axis (horizontal) by five superstructure reflections. Diffuse scattering is observed around the Bragg peaks. The intensities are rescaled to the interval 0 (white) to 100 (black); the stronger peaks are clipped (highest intensity in this figure: over 64 000 counts per pixel).

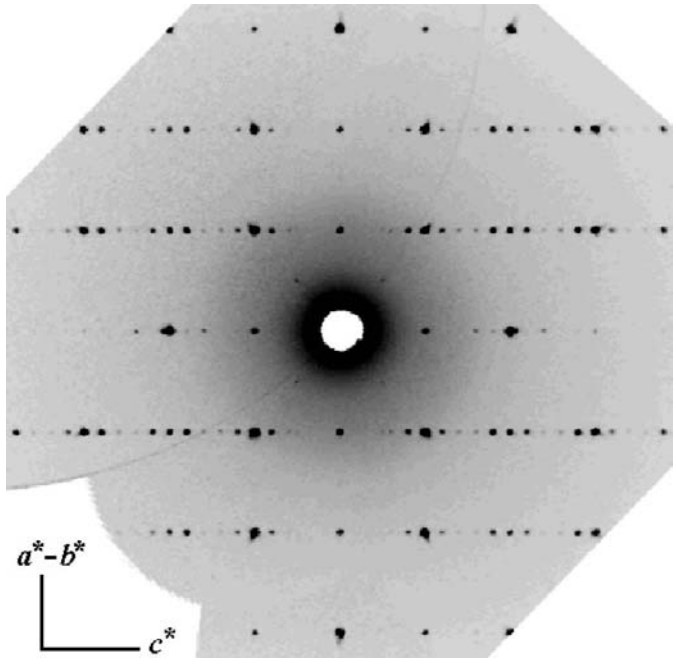

Figure 4
Reconstructed image of the ($h\bar{h}0l$) reciprocal plane of the fivefold superstructure of CaAlSi. The strong reflections correspond to the average structure with the symmetry $P6/mmm$; they are separated along the c^* axis (horizontal) by four superstructure reflections. The weak ($\frac{1}{2}\frac{\bar{1}}{2}\frac{\bar{5}}{2}$), ($\frac{1}{2}\frac{1}{2}\frac{5}{2}$), ($\frac{\bar{1}}{2}\frac{1}{2}\frac{5}{2}$) and ($\frac{\bar{1}}{2}\frac{\bar{1}}{2}\frac{\bar{5}}{2}$) reflections around the centre of the image are due to the $\lambda/2$ radiation. The intensities are rescaled to the interval 0 (white) to 100 (black); the stronger peaks are clipped (highest intensity in this figure: over 64 000 counts per pixel).

Table 3
Positional deviations (%) from the average $P6/mmm$ structure, $2|z_0 - z|/z_0 + z$, where z_0 is the expected position from the average structure, rescaled within the supercell, and z is the refined position taking into account the superstructure reflections.

Sixfold superstructure:			1st layer		2nd layer		3rd layer		4th layer	
Ca1	Ca2	Ca3	Si1	Si2	Si3	Si4	Si5	Si6	Si7	Si8
1.6 (1)	0.29 (6)	0.15 (3)	0	0	3.8 (1)	2.6 (1)	1.61 (5)	2.34 (7)	0	0
Fivefold superstructure:			1st layer		2nd layer		3rd layer			
Ca1	Ca2	Ca3	Si1	Si2	Si3	Si4	Si5	Si6		
0	0.30 (4)	0.31 (1)	13.1 (1)	5.41 (8)	2.73 (3)	2.98 (4)	0	0		

Table 4
Sixfold superstructure of CaAlSi (three-dimensional refinement): selected interatomic distances and angles.

Distances (Å)		Angles (°)	
(Si,Al)1—(Si,Al)2	2.41170 (2)†	(Si,Al)2—(Si,Al)1—(Si,Al)2	120
(Si,Al)3—(Si,Al)4	2.4279 (7)	(Si,Al)4—(Si,Al)3—(Si,Al)4	118.69 (5)
(Si,Al)5—(Si,Al)6	2.4367 (9)	(Si,Al)6—(Si,Al)5—(Si,Al)6	118.00 (7)
(Si,Al)7—(Si,Al)8	2.41170 (2)†	(Si,Al)8—(Si,Al)7—(Si,Al)8	120
(Si,Al)1—(Si,Al)3	4.225 (5)		
(Si,Al)2—(Si,Al)4	4.504 (5)		
(Si,Al)3—(Si,Al)5	4.411 (5)		
(Si,Al)4—(Si,Al)6	4.479 (8)		
(Si,Al)5—(Si,Al)7	4.527 (4)		
(Si,Al)6—(Si,Al)8	4.179 (6)		
Ca1—Ca1^{i}	4.320 (7)		
Ca1—Ca2	4.402 (5)		
Ca2—Ca3	4.423 (5)		
Ca3—Ca3^{ii}	4.355 (7)		

Symmetry codes: (i) $x, y, -z$; (ii) $x, y, -z+1$. † $a/3^{1/2}$.

Table 5
Fivefold superstructure of CaAlSi (three-dimensional refinement): selected interatomic distances and angles.

Distances (Å)		Angles (°)	
(Si,Al)1—(Si,Al)2	2.4431 (5)	(Si,Al)2—(Si,Al)1—(Si,Al)2	117.49 (4)
(Si,Al)3—(Si,Al)4	2.4407 (4)	(Si,Al)4—(Si,Al)3—(Si,Al)4	117.68 (3)
(Si,Al)5—(Si,Al)6	2.41170 (2)†	(Si,Al)6—(Si,Al)5—(Si,Al)6	120
(Si,Al)1—(Si,Al)1^{i}	3.846 (5)		
(Si,Al)1—(Si,Al)3	4.481 (2)		
(Si,Al)2—(Si,Al)2^{i}	4.631 (3)		
(Si,Al)2—(Si,Al)4	4.465 (2)		
(Si,Al)3—(Si,Al)5	4.565 (2)		
(Si,Al)4—(Si,Al)6	4.188 (3)		
Ca1—Ca2	4.375 (2)		
Ca2—Ca3	4.428 (2)		
Ca3—Ca3^{ii}	4.332 (2)		

Symmetry codes: (i) $x, y, -z$; (ii) $x, y, -z+1$. † $a/3^{1/2}$.

not trivial because of pseudosymmetry effects and the systematic relative weakness of many superstructure reflections.

In both cases, the structures were constructed from the average $P6/mmm$ structure and refined in all the hexagonal and trigonal space groups matching the observed reflection conditions (none). The space groups not allowing corrugated (Al,Si) layers (where the special positions $\frac{1}{3}, \frac{2}{3}, z$ and $\frac{2}{3}, \frac{1}{3}, z$ are equivalent) were discarded because they did not lead to satisfactory reliability factors. However, the comparisons between the qualities of the best refinements were too ambiguous to determine the correct symmetries. We then performed many refinements in the space group $P1$ with different starting corrugations for the (Al,Si) layers, allowing only the z coordinates of the atoms to move as is the case in the hexagonal and trigonal space groups. These refinements always converged towards the same configurations with two flat layers for the sixfold superstructure and with one flat layer for the fivefold superstructure, the other layers showing different degrees of corrugation.

We retained in both cases the space group $P\bar{6}m2$ (No. 187) as the highest-symmetry space group leading to a good quality refinement and keeping the (Al,Si) layer corrugation pattern observed from the triclinic refinements (Tables 3, 4 and 5; Figs. 5, 6 and 7). Each layer contains two crystallographically different (Al,Si) sites. It should be noted that for the description of the sixfold superstructure in the space

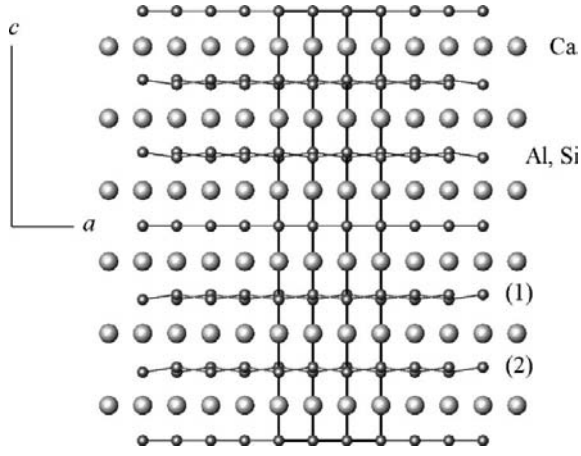

Figure 5
Sixfold superstructure of CaAlSi: the corrugated (Al,Si) layers.

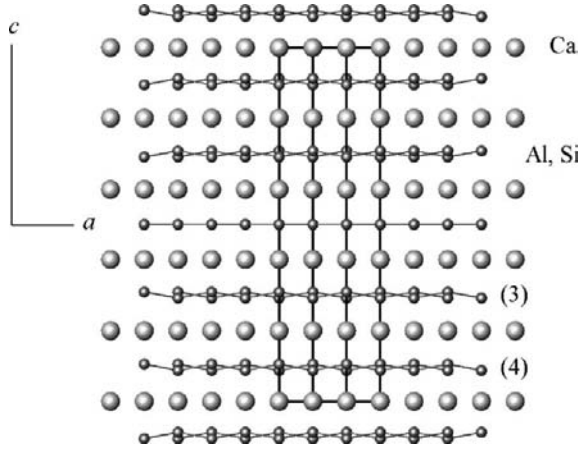

Figure 6
Fivefold superstructure of CaAlSi: the corrugated (Al,Si) layers.

Table 6
Reflection details for the (3 + 1)-dimensional indexations.

The unit-cell parameters are $a = 4.17720$ Å and $c_0 = 4.38744$ Å; the modulation vectors $\mathbf{q}_6 = (0, 0, 1/6)$ and $\mathbf{q}_5 = (0, 0, 1/5)$ were used.

	Sixfold modulation		Fivefold modulation	
(*hklm*) range	±5, ±5, ±5, ±3		±5, ±5, ±6, ±2	
Total amount of reflections	$I > 3\sigma$	All	$I > 3\sigma$	All
Main reflections ($m = 0$)	443	470	831	873
Satellites $m = 1$	570	1049	1154	1939
Satellites $m = 2$	97	1070	517	1907
Satellites $m = 3$	0	545	–	–

group $P\bar{6}m2$, the change of the origin (Al and Si in the mirror planes at $z = 0$ and $z = \frac{1}{2}$ instead of Ca), necessary to obtain the right corrugation pattern, results in better reliability factors; also, when transformed into the space group $P1$ and refined, the model with Ca in the mirror planes automatically converges towards the $P\bar{6}m2$ solution with (Al,Si) in the mirror planes.

Since it is not possible to distinguish properly between the Al and Si atoms by means of X-ray diffraction, their positions were refined on the same sites, with the same anisotropic displacement parameters for each site and occupations of 50%. The final Fourier maps do not indicate the presence of O atoms within the structure.

3.2.2. Description in (3 + 1) dimensions. Since the intensities of the satellite reflections decrease strongly as their order increases, a description of the structures using a superspace approach seems more appropriate.

The basic structures of both phases (AlB_2-type, $P6/mmm$) were first refined with the program *SHELXL97* (Fig. 8). The elongation of the atomic displacement tensors along the *c* axis for the (Si,Al) atoms is more pronounced in the case of the fivefold superstructure than the sixfold superstructure ($U^{33}/U^{11} = 6.2$ and 4.7, respectively).

For the (3 + 1)-dimensional indexings, we chose the modulation vectors $\mathbf{q}_6 = 1/6\mathbf{c}_0^*$ and $\mathbf{q}_5 = 1/5\mathbf{c}_0^*$ (the subscripts refer to the six- and fivefold superstructure, respectively). In both phases, the first-order satellite reflections have higher intensities than the other order satellites (Table 6). From the results of the three-dimensional refinements and using the program *SUPERSPACE GROUP FINDER* (Orlov & Chapuis, 2005), we chose as possible superspace groups those that lead to the supercell space group $P\bar{6}m2$: $P\bar{6}m2(00\gamma)$, $P\bar{6}m2(00\gamma)0s0$, $P6/mmm(00\gamma)s00s$ and $P6_3/mmc(00\gamma)$. However, since there are no reflection conditions, the only suitable superspace group is $P\bar{6}m2(00\gamma)$. This choice is also in agreement with the fact that the external part of the (3 + 1)-dimensional point group must be equal to or a subgroup of the point group $6/mmm$ of the basic structure (Yamamoto & Nakazawa, 1982; Janssen *et al.*, 1999).

The chosen global phase parameters were $\delta = 0$ for both superstructures (see further in the text). The refinements were performed with the calculated weighting scheme $w = 1/\sigma^2(F_0)$. The starting model for the sixfold modulated structure contains one Ca atom at 0, 0, $\frac{1}{2}$ and two mixed (Al,Si) sites at $\frac{1}{3}, \frac{2}{3}, 0$ and $\frac{2}{3}, \frac{1}{3}, 0$; because of the symmetry, these positional parameters are not refinable. The basic structure was first refined using only the main reflections; then the first-order displacive modulation functions were added for all atoms and refined using the main reflections and the $m = 1$ and $m = 2$ reflections. Because their intensities are too weak (Table 6), the $m = 3$ satellites were not used. In order to assure convergence to the global minimum, all possible sign

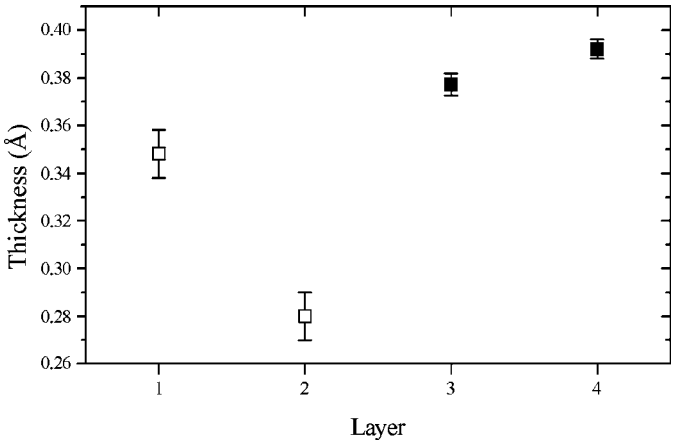

Figure 7
Thicknesses of the different corrugated layers in CaAlSi. The labelling of the layers is defined in Figs. 5 and 6. The empty squares correspond to the sixfold superstructure and the filled squares to the fivefold superstructure. The values for the flat layers (0 Å) are not shown for clarity.

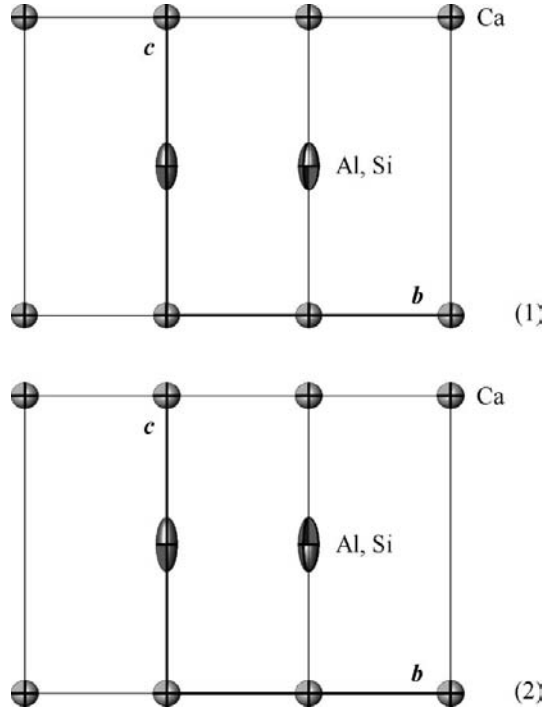

Figure 8
Basic structure of CaAlSi: Anisotropy of the atomic displacement parameters for Al and Si. (1) Refinement from the main reflections of the sixfold superstructure. (2) Refinement from the main reflections of the fivefold superstructure.

Table 7
Final R values for the (3 + 1)-dimensional refinements.

Sixfold superstructure: 19 parameters Reflections group	R_{obs}	R_{all}	wR_{obs}	wR_{all}
All	0.0409	0.0981	0.0651	0.0732
$m = 0$	0.0309	0.0361	0.0607	0.0691
$m = 1$	0.0583	0.1270	0.1381	0.1417
$m = 2$	0.619	0.4533	0.3233	0.4950
Fivefold superstructure: 21 parameters				
Reflections group	R_{obs}	R_{all}	wR_{obs}	wR_{all}
All	4.84	9.55	6.98	7.06
$m = 0$	3.16	3.29	6.42	6.42
$m = 1$	6.09	11.88	10.68	10.92
$m = 2$	13.91	32.00	33.75	41.71

Table 8
Sixfold modulated structure of CaAlSi: displacive modulation amplitudes (fractional coordinates), atomic displacement parameters (Å^2) and their modulation amplitudes (Å^2).

	(Al,Si)1	(Al,Si)2	Ca
$z$sin 1	0.036 (2)	−0.045 (2)	−0.004 (2)
$z$sin 2	−0.014 (2)	−0.004 (2)	−0.005 (1)
U^{11}	0.006 (2)	0.012 (2)	0.0137 (3)
U^{33}	0.034 (4)	0.034 (4)	0.0127 (4)
U^{12}	0.0030 (8)	0.0061 (8)	0.0068 (1)
U^{11}cos 1	0†	0.0053 (9)	–
U^{33}cos 1	−0.029 (3)	0.026 (3)	–
U^{12}cos 1	0†	0.0027 (4)	–
U^{11}cos 2	0†	−0.003 (2)	–
U^{33}cos 2	0.010 (4)	0.016 (4)	–
U^{12}cos 2	0†	−0.002 (1)	–

† Values smaller than their standard deviation were set to 0 for the last refinement cycles.

Table 9
Fivefold modulated structure of CaAlSi: displacive modulation amplitudes (fractional coordinates), atomic displacement parameters (Å^2) and their modulation amplitudes (Å^2).

	(Al,Si)1	(Al,Si)2	Ca
$z$sin 1	0.0472 (8)	−0.0581 (7)	−0.0012 (5)
$z$sin 2	0.0010 (6)	−0.0311 (6)	−0.0054 (4)
U^{11}	0.0040 (5)	0.0154 (5)	0.0152 (1)
U^{33}	0.041 (1)	0.0306 (8)	0.0135 (1)
U^{12}	0.0020 (2)	0.0077 (3)	0.00762 (7)
U^{11}cos 1	0.0029 (5)	0.0084 (7)	–
U^{33}cos 1	−0.032 (1)	0.017 (1)	–
U^{12}cos 1	0.0014 (2)	0.0042 (3)	–
U^{11}cos 2	−0.0070 (6)	0.0012 (9)	–
U^{33}cos 2	0.017 (1)	0.005 (1)	–
U^{12}cos 2	−0.0035 (3)	0.0006 (4)	–

combinations for the amplitudes of the modulation functions were tested. There again, because of the weak anomalous dispersion of the material, a simultaneous change of all the signs of the modulation amplitudes does not yield different results. Second-order parameters were then refined; the amplitudes of the deviation functions for the Ca atom were much lower than for the (Si,Al) atoms and barely significant. This result is consistent with the three-dimensional description: The Ca atoms do not deviate much from their ideal positions (Table 3). Finally, the parameters for the modulation functions of the atomic displacement parameters up to second order were refined for the (Al,Si) atoms, which still improved the R values but mostly for the second-order satellites (Tables 7 and 8). The starting model for the fivefold modulated structure contains one Ca atom at $0, 0, 0$ and two mixed (Al,Si) sites at $\frac{1}{3}, \frac{2}{3}, \frac{1}{2}$ and $\frac{2}{3}, \frac{1}{3}, \frac{1}{2}$. We applied the same refinement procedure as for the sixfold modulated structure, except that, in the case of the Ca atom, the refinement of second-order displacive parameters led to more significant values and greatly improved the R values of the $m = 2$ satellites (Tables 7 and 9). In both the six- and the fivefold modulated structures, the anisotropy of the atomic displacement tensors is reduced but still remains at the end of the refinement.

From the results of the refinements, we see that both the three-dimensional and the (3 + 1)-dimensional descriptions are suitable to describe the modulations in CaAlSi. Also, the (Al,Si)–(Al,Si) distances within each layer from the three-dimensional refinements compare well with the distances from the (3 + 1)-dimensional refinements, within three standard deviations (Figs. 9 and 10). Finally, while the correlations are weak for the three-dimensional refinements (Table 2), the (3 + 1)-dimensional refinements give rise to a strong correlation between the U^{11} parameters of the two (Al,Si) atoms, although the number of refined parameters is reduced: the most important correlation coefficient is −0.964 for the sixfold modulated structure and −0.960 for the fivefold modulated structure.

In the case of commensurately modulated structures, the global phase parameter δ, corresponding to the t-section value defining the real three-dimensional space group of the supercell structure and denoted t_0 in the *JANA2000* program, affects the quality of the refinement (Yamamoto & Nakazawa, 1982). For the sixfold modulated structure, the particular values $\delta = n/6$ and $\delta = 1/12 + n/6$ lead to the supercell space group $P\bar{6}m2$, while all other values lead to $P3m1$. For the fivefold modulated structure, only $\delta = n/5$ and $\delta = 1/10 + n/5$ lead to $P\bar{6}m2$. On the other hand, the choice of any δ for incommensurate structures should not influence the quality of the refinement. For both structures, comparative refinements were performed for different values of δ (Table 10). The results for the fivefold superstructure show that the modulations are truly commensurate and validate the initial choice of $\delta = 0$ as well as the choice of the supercell space group $P\bar{6}m2$, at least *versus* $P3m1$. Comparative refinements for the sixfold superstructure (Table 10) do not allow such an unequivocal determination. From the R values, the model with $\delta = 1/12 + n/6$ seems to be the best description; however, it corresponds to the three-dimensional model in space group $P\bar{6}m2$ with Ca atoms in the mirror planes at $z = 0$ and $z = \frac{1}{2}$. Refinements with *SHELXL97* have shown that this model leads to less satisfactory R values and a qualitatively different corrugation pattern for the (Al,Si) layers than the chosen model with (Al,Si) sites in the mirror planes, corresponding to $\delta = 0$. It should also be noted that the qualities of the (3 + 1)-dimensional refinements differ only

Table 10
Choice of the global phase parameter δ: R_{obs} from comparative refinements.

Sixfold modulation: 19 parameters					
δ	Overall	Main	$m=1$	$m=2$	Supercell space group
$n/6$	4.09	3.09	5.83	16.19	$P\bar{6}m2$
$1/48+n/6$	4.08	3.09	5.85	15.52	$P\bar{3}m1$
$1/24+n/6$	4.06	3.07	5.88	14.06	$P\bar{3}m1$
$3/48+n/6$	4.04	3.06	5.89	13.14	$P\bar{3}m1$
$1/12+n/6$	4.02	3.05	5.88	12.95	$P\bar{6}m2$
Incommensurate Refinement	4.05	3.07	5.85	13.92	–

Fivefold modulation: 21 parameters					
δ	Overall	Main	$m=1$	$m=2$	Supercell space group
$n/5$	4.84	3.16	6.09	13.91	$P\bar{6}m2$
$1/40+n/5$	5.42	3.19	6.73	19.34	$P\bar{3}m1$
$1/20+n/5$	6.14	3.08	7.67	26.40	$P\bar{3}m1$
$3/20+n/5$	6.11	3.06	7.58	26.60	$P\bar{3}m1$
$1/10+n/5$	5.76	3.13	6.72	24.96	$P\bar{6}m2$

very slightly, except for the relatively small set of the weak $m=2$ satellite reflections – the highest I/σ ratio for the second-order satellites is 10.8. Given the limited accuracy of the diffraction data for the sixfold superstructure, we are left with the problem that just a few weak second-order satellites do not unequivocally fix the global phase parameter δ. We chose the (3 + 1)-dimensional commensurate description with $\delta=0$ in order to keep the consistency with the three-dimensional model.

4. Discussion

The main feature of both structures is the stacking of differently puckered (Al,Si) layers along the *c* axis (Figs. 5, 6 and 7). Puckered graphite-like layers have already been observed in many compounds with AlB_2-type related structures, such as for instance in the gallides LiGaGe (Bockelmann & Schuster, 1974), CaGaGe and SrGaSn (Czybulka *et al.*, 1989) or the metastable phase $MgGa_2$ (Ellner *et al.*, 1980), but in these cases the deviation from planarity is the same in every layer. In most AlB_2-related compounds with corrugated nets, the aplanarity is directly connected to an ordering of the two different species within the net. In some compounds – specifically those with small 'spacers' (such as Li) – the distance between the layers is so small that covalent interactions between the layers begin to play a role, which further contributes to the corrugation of the layers (see for instance Hoffmann & Pöttgen, 2001). This is obviously not the case for CaAlSi (Tables 4 and 5): The shortest inter-layer (Si,Al)–(Si,Al) distances are 4.179 (6) Å for the sixfold superstructure and 3.846 (5) Å for the fivefold superstructure – not enough for any sizable covalent interaction. The reason for a modulation of the corrugation in CaAlSi is as yet unclear.

One possibility could be a spatial variation of the charge transfer from the Ca atoms to the (Si,Al) layers which could, in turn, influence the corrugation. The ground state of the crystal would then represent a delicate balance between the energy gain and expense involved in modulating the net charge and the deformation of the (Si,Al) layers. This 'electronic explanation' would have considerable implications for the interpretation of superconductivity in CaAlSi. However, the fact that the modulation does not change with temperature (below room temperature) and the observation that it apparently depends on the sample's thermal history at high temperatures (see above) seem to contradict this hypothesis.

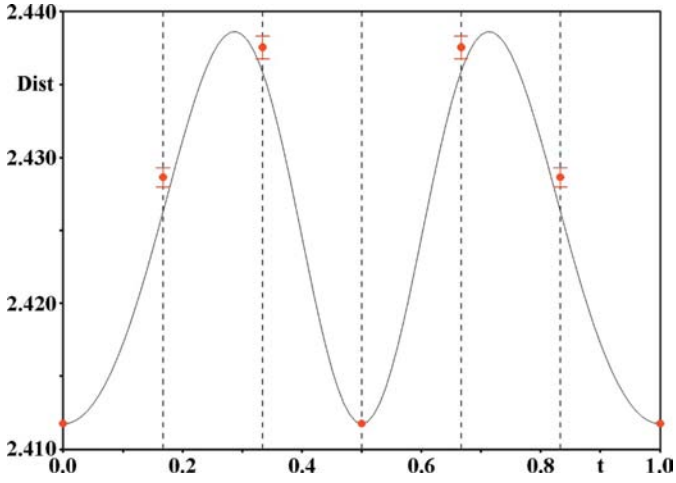

Figure 9
(3 + 1)-dimensional refinement (*JANA*2000) of the sixfold modulated structure of CaAlSi: (Al,Si)—(Al,Si) distances within the layers as a function of the additional coordinate *t*. The dashed vertical lines show the commensurate sections corresponding to the layers in the three-dimensional supercell. The distances from the three-dimensional refinements (*SHELXL*97) are indicated for each section with their standard deviations.

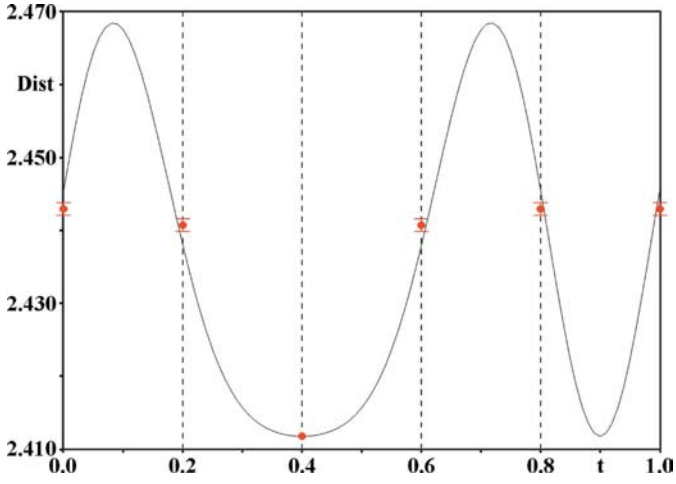

Figure 10
(3 + 1)-dimensional refinement (*JANA2000*) of the fivefold modulated structure of CaAlSi: (Al,Si)—(Al,Si) distances within the layers as a function of the additional coordinate *t*. The dashed vertical lines show the commensurate sections corresponding to the layers in the three-dimensional supercell. The distances from the three-dimensional refinements (*SHELXL97*) are indicated for each section with their standard deviations.

At least, the energy scale of the process leading to the modulated corrugation is very different from that of superconductivity in CaAlSi.

Instead, we favour the scenario of a partial ordering of Si and Al along the stacks of corrugated nets. Different corrugations would imply different Si:Al ratios and/or different degrees of local order, and also possibly different electron counts on the nets. In this description, the samples studied at room temperature and below would represent 'stranded structures', which are products of a kinetically hindered ordering or exsolution process occurring during fast cooling from the preparation temperature. Depending on the thermal history, different ordering states develop, resulting in the two distinct long-range ordered superstructures (fivefold and sixfold) observed so far.

However, we can also not completely exclude the possibility that traces of oxygen within the crystals may influence the polymorphism of CaAlSi.

Along with the overall stoichiometry of individual layers, the degree of Si–Al ordering within the layers will be an important parameter that needs to be characterized. Unfortunately, both are virtually inaccessible by our X-ray diffraction experiments: We can only detect the corrugation that results from the proposed partial ordering of Si and Al, not the ordering itself. Powder neutron and NMR measurements are currently planned – once strictly single-phase samples are available – to gain further insight into these phenomena.

5. Conclusions

We have found and characterized a novel form of modulated corrugations of the (Si,Al) graphite-like nets in crystals of the superconductor CaAlSi. In contrast to all AlB_2-related compounds known so far, the corrugation of the nets varies from one layer to the next. The reason for the observed polymorphism is as yet unclear. The resulting complex superstructures and the closely related local disorder in CaAlSi have important implications for a better understanding of superconductivity in these compounds. Further preparative and analytical work is needed to characterize this interesting material completely.

References

Bockelmann, W. & Schuster, H.-U. (1974). *Z. Anorg. Allg. Chem.* **410**, 233–240.

Bordet, P., Affronte, M., Sanfilippo, S., Núñez-Regueiro, M., Laborde, O., Olcese, G. L., Palenzona, A., LeFloch, S., Levy, D. & Hanfland, M. (2000). *Phys. Rev. B*, **62**, 11392–11397.

Czybulka, A., Pinger, B. & Schuster, H.-U. (1989). *Z. Anorg. Allg. Chem.* **579**, 151–157.

Dowty, E. (2000). *ATOMS for Windows*. Version 5.1. Shape Software, Kingsport, Tennessee, USA.

Ellner, M., Gödecke, T., Duddek, G. & Predel, B. (1980). *Z. Anorg. Allg. Chem.* **463**, 170–178.

Farrugia, L. J. (1999). *J. Appl. Cryst.* **32**, 837–838.

Flack, H. D. (1983). *Acta Cryst.* A**39**, 876–881.

Hardy, G. F. & Hulm, J. K. (1954). *Phys. Rev.* **93**, 1004–1016.

Hoffmann, R.-D. & Pöttgen, R. (2001). *Z. Kristallogr.* **216**, 127–145.

Imai, M., Nishida, K., Kimura, T. & Abe, H. (2002). *Physica C*, **377**, 96–100.

Imai, M., Nishida, K., Kimura, T., Kitazawa, H., Abe, H., Kitô, H. & Yoshii, K. (2002). *Physica C*, **382**, 361–366.

Janssen, T., Janner, A., Looijenga-Vos, A. & de Wolff, P. M. (1999). *International Tables for Crystallography*, edited by A. J. Wilson & E. Prince, pp. 899–947. Dordrecht, The Netherlands: Kluwer Academic Publishers.

Lorenz, B., Lenzi, J., Cmaidalka, J., Meng, R. L., Sun, Y. Y., Xue, Y. Y. & Chu, C. W. (2002). *Physica C*, **383**, 191–196.

MacWhan, D. B., Compton, V. B., Silverman, M. S. & Soulen, J. R. (1967). *J. Less-Common Met.* **12**, 75–76.

Nagamatsu, J., Nakagawa, N., Muranaka, T., Zenitani, Y. & Akimitsu, J. (2001). *Nature* (*London*), **410**, 63–64.

Orlov, I. & Chapuis, G. (2005). Superspace Tools. http://superspace.epfl.ch.

Petricek, V., Dusek, M. & Palatinus, L. (2000). *JANA2000.* Institute of Physics, Czech Academy of Sciences, Prague, Czech Republic.

Rodriguez-Carvajal, J. (2005). *Fullprof.* Version June 2005. LLB, CEA/Saclay, France.

Sanfilippo, S., Elsinger, H., Núñez-Regueiro, M., Laborde, O., LeFloch, S., Affronte, M., Olcese, G. L. & Palenzona, A. (2000). *Phys. Rev. B*, **61**, R3800–R3803.

Sheldrick, G. M. (1997). *SHELX97.* University of Göttingen, Germany.

Stoe & Cie (1996). *X-SHAPE and X-RED*. Stoe and Cie GmbH, Darmstadt, Germany.

Stoe & Cie (2002). *X-AREA*. Stoe & Cie GmbH, Darmstadt, Germany.

Tamegai, T., Uozato, K., Ghosh, A. K. & Tokunaga, M. (2005). *Int. J. Mod. Phys. B*, **19**, 369–374.

Yamamoto, A. & Nakazawa, H. (1982). *Acta Cryst.* A**38**, 79–86.